PCCP

ARTICLE TYPE

Cite this: DOI: 00.0000/xxxxxxxxxx

Histone H3 as a redox switch in the nucleosome core particle: insights from molecular modeling†

Yasaman Karami,[a‡] Roy González-Alemán,[b‡] Mailys Duch,[b] Yuya Qiu,[b] Yani Kedjar,[b] and Emmanuelle Bignon*[b]

Received Date
Accepted Date

DOI: 00.0000/xxxxxxxxxx

Histones post-translational modifications are major regulators of the chromatin dynamics. Understanding the structural signature of these marks in the nucleosome context is of major importance to unravel their mechanisms of action and open perspectives for the development of new therapies. In this work, we rely on multi-microseconds molecular dynamics simulations and advanced structural analysis to unravel the effect of two modifications of the histone H3: S-sulfenylation and S-nitrosylation. These oxidative modifications are known to target the cysteine 110 on the histone H3, but there their effect on the nucleosome dynamics. In this study, we show that in a nucleosome core particle, S-sulfenylation and S-nitrosylation exhibit different structural signatures, which suggests that they play a different function. While S-sulfenylation destabilizes DNA-histone communication at the dyad and could be linked to the promotion of nucleosome disassembly events, S-nitrosylation exhibits a mild effect on the nucleosome dynamics and might have a different function. Our results highlight the fine tune link between the chemical nature of histone core post-translational modifications and their impact on the nucleosome's large architecture. We provide new insights into the regulatory mechanisms of histone oxidative modifications, about which very little is known so far.

Introduction

In cells, DNA is tightly compacted by histone proteins to fit into the nucleus. At the first level of compaction, the so-called nucleosome, the double helix is wrapped onto an octamer of histone proteins[1] - see Figure 1-a. The histone core is made up of two copies of four types of histones (H3, H4, H2A, and H2B), each of which exhibits an N-terminal disordered tail that protrudes from the nucleosome core particle (NCP). Of note, H2A also has a disordered C-terminal tail.

DNA compaction is a dynamic phenomenon that is regulated by a plethora of epigenetic factors. Among them, post-translational modifications (PTMs) of histone proteins are crucial, and hundreds of them have been characterized to date[3]. They are known to regulate the dynamics of the nucleosome through highly complex mechanisms that remain ill-defined in many ways. Large

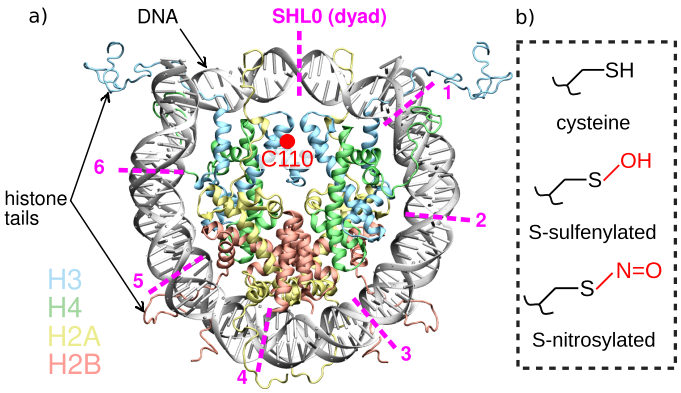

Fig. 1 a) Structure of a nucleosome core particle, composed of 145 DNA base pairs wrapped onto an octamer of histone proteins (H3 in blue, H4 in green, H2A in yellow, H2B in orange). Super helical locations are indicated in magenta with the dyad considered as SHL0. A red dot locates histone H3 cysteine 110, which can undergo oxidative modifications in the nucleosome. Adapted from Gillet et al[2]. b) Structure of a canonical cysteine (top) and its S-sulfenylated (center) and S-nitrosylated (bottom) derivatives.

[a] Université de Lorraine, CNRS, Inria, LORIA, F-54000 Nancy, France
[b] Université de Lorraine and CNRS, UMR 7019 LPCT, F-54000 Nancy, France; E-mail: emmanuelle.bignon@univ-lorraine.fr

† Electronic Supplementary Information (ESI) available: details and results of the COMMA2 analysis and supplementary figures (Full view of binding pockets on the nucleosome; DNA/histones flexibility profiles including S-sulfonylation; Projection of the histone tails conformations; Curves+ descriptors; Projection of the communities generated by ComPASS; Hydrogen Bond mapping of native DNA-histone interactions. See DOI: 10.1039/cXCP00000x/

‡ These authors contributed equally to this work.

amounts of investigations have been focused on histone PTMs located on the histone tails, which can exhibit a direct effect on DNA/tails electrostatic interactions but can also influence the binding of partner proteins such as chromatin factors. The high complexity of the mechanisms of action associated with histone PTMs is further illustrated by their possible combinatorial effects and the fact that one amino acid can participate to different processes depending on the nature of the modification it undergoes. For instance, H3K9 methylation is well known to promote chromatin compaction via its specific binding to the HP1 protein, while its acetylation participates to chromatin opening via direct perturbation of interactions with the DNA. Besides, the crosstalk between H3S10 phosphorylation and H3K9 acetylation has been highlighted as H3S10ph can block H3K9 methylation.

Regarding PTMs located on the histone core, numerous have been investigated and new ones are frequently discovered. An extensive body of experimental studies have suggested that modifications would either promote nucleosome disassembly when located near the dyad, or favor DNA unwrapping if positioned on the histone core lateral surface[4]. For instance, H3T118 phosphorylation or H3K64 acetylation near the dyad destabilize the nucleosome structure[5,6], while H4K77 or H3K56 acetylation located on the sides promote DNA unwrapping[4]. Nevertheless, there is a lack of structural data to fully understand these regulatory mechanisms at the atomic scale.

Such a lack of data is especially marked for oxidative PTMs, which target mainly cysteine residues of proteins, and are well known to regulate a large panel of proteins in cells and to be deregulated in many diseases. For instance, S-nitrosylation is well known to play a crucial role in many different signaling pathways, which are deregulated upon cancer onset and progression (e.g., proliferation, apoptosis)[7,8]. While it can result from the reaction between the cysteine's sulfur atom with nitric oxide or with low molecular weight -NO donor (e.g. GSNO), enzymes catalyzing protein (de-)nitrosylation are also known to target a wide range of proteins[9,10]. This is the case for insulin receptors, which are found to be nitrosylated by the recently discovered SCAN enzyme[11]. S-sulfenylation is formed by reaction between the cysteine and reactive oxygen species (e.g. H_2O_2), and is also involved in the modulation of a plethora of proteins activity. It is well known as a major redox sensor influencing many signaling pathways[12] with, for instance, a role in the regulation of protein folding[13] and in vascular homeostasis maintenance[14]. Some irreversible oxidative PTMs such as S-sulfonylation are also markers of oxidative stress and can promote protein degradation[15,16].

In the nucleosome context, the histone H3 cysteine 110 is known to undergo different types of oxidative modifications[17,18]. Experimental studies have shown that H3C110 S-gluthationylation promotes chromatin opening[19] and is linked to cell proliferation[20], while some of our recent computational works underlined the possible promotion of the nucleosome disassembly by S-sulfonylation[21]. While computational studies of the nucleosome dynamics and the effects of some mainstream PTMs have been released[22–27], there is a drastic lack of theoretical research concerning oxidative PTMs.

In this work, our aim is to palliate this lack of data by investigating two histone oxidative modifications: H3C110 S-sulfenylation and S-nitrosylation (see Figure 1-b). We performed extensive MD simulations to probe their effect on the structural and dynamic properties of a nucleosome core particle (NCP). The exploitation of 20 μs unbiased molecular dynamics (MD) simulations highlight different impact of the two PTM. S-sulfenylation strongly perturbs the histone-DNA interactions, favoring DNA breathing/unwrapping and destabilizing the dyad, while S-nitrosylation exhibits a much milder effect solely featuring a slight promotion of DNA breathing. These results point to a differential function of these two PTMs in the nucleosome: S-sulfenylation destabilization of the dyad might participate to nucleosome disassembly processes, while S-nitrosylation might act as a reaction intermediate (e.g. towards S-glutathionylation) or be functional only in combination with other PTMs.

Computational Methods

All MD simulations were performed with the AMBER20 suite of programs, while the VMD[28] and Pymol[29] software were used for visualization and figures rendering.

Systems setup

Starting systems were built from the crystal structure of the nucleosome core particle featuring an α-satellite DNA sequence and full histone tails (PDB ID 1KX5[30]). The three missing residues (PEP) at the N-terminus of both H2B copies were reconstructed using VMD. Nitrosylation and sulfenylation were introduced on the first copy of H3C110 using the leap functionality of AMBER, which did not create any clash contact. The AMBER ff14SB force field[31] was used in combination with bsc1[32] and the CUFIX[33] corrections for non-bonded terms. Parameters for the sulfenylated cysteine were generated in house as described in previous work[21], and those of the nitrosylated cysteine were taken from the literature[34].

Each modified system, i.e. with nitrosylation (named 1KX5+SNO) or with sulfenylation (named 1KX5+SOH), was placed into a TIP3P water box with a truncated octahedron shape using a buffer of 20Å. The addition of 434 Na^+ and 288 Cl^- ions ensured the neutrality and a salt concentration of 0.150M, resulting in systems of ∼427,000 atoms.

Molecular dynamics protocol

The starting structures were first optimized in 4 steps with decreasing position restraints on the nucleosome core particle atoms from 20 kcal/mol to 5 kcal/mol. For each one of these 4 steps, a minimization run of 10,000 steps (with the steepest descent switched to conjugate gradient after 5,000 steps) was followed by a short equilibration run of 20 ps at 100K. This procedure allows the structure to be smoothly optimized in its environment. A final 10,000 steps minimization without restraint was then followed by 20 ps thermalization to increase the temperature to 300K and a 500 ps equilibration in NVT to equilibrate the solvent. The system was then relaxed in NPT during 100 ns before a 2 μs production run. The latter was performed using a 4 fs timestep allowed by the use of the HMR approach on the protein and DNA atoms[35,36].

Temperature and pressure were kept constant (300K, 1 bar) using the Langevin thermostat with a 2 ps^{-1} collision frequency and the Berendsen barostat with isotropic position scaling and a pressure relaxation time of 1 ps. A classical 8 Å cutoff was used for non-bonded terms, and long-range electrostatics were treated using the Particle Mesh Ewald approach[37]. Bonds involving hydrogen were constrained using the SHAKE algorithm. For each system, five replicates were produced with random starting velocities, resulting in a total of 20 μs of sampling.
Control MD ensembles (6x2 μs) for the unmodified nucleosome core particle were taken from a previous work[21].

Structural analyses

The flexibility analysis was performed using a PCA-based python script that we successfully applied on other nucleosomal systems[21,38,39]. It uses the inverse distance between each pair of residues as internal coordinates, extracted directly from the MD trajectories. The eigenmodes and eigenvectors of the generated covariance matrix can be interpreted as the primary modes of motion and their amplitude. We can then determine how much each residue contributes to the system's overall flexibility by analyzing the per residue contribution to these motions.
DNA structural descriptors were computed using the Curves+ program[40]. We performed the analyses for all base pairs and all descriptors provided by Curves+.
The ComPASS tool was used to identify communication network of each nucleosome system. Starting from the MD trajectories of a given system, ComPASS extracts the following properties to build an adjacency matrix: generalized correlations, non-covalent interactions, communication propensity (variance of inter-residue distances), and inter-residue distances. Then we build a graph, where nodes are amino acids and/or nucleotides, and edges are constructed by applying a distance cutoff to the average minimum distance matrix. The adjacency matrix is then used to assign weights to the graph. Finally, we identify the following notions from the graph: *i)* shortest pathways between every pair of residues, *ii)* hotspots (based on centrality measures), *iii)* cliques (fully connected groups of residues) and *iv)* communities (highly interconnected groups of residues that may have a common functional role).
To track the progress of molecular interactions between DNA and the histone octamer, we utilized the ProLIF software[41]. The program's default geometrical definitions were applied to the trajectories using 10-frame steps. We observed several types of contacts between different moieties, including anionic, hydrogen bonding (acceptor and donor), π-cation, π-stacking, hydrophobic, and Van-der-Waals. Two residues were considered interacting if, in more than 20% of the frames considered, any of the contacts mentioned above were detected between them. As this study focuses on re-organization of the histone core upon oxidation, we excluded the histone tails from the DNA-protein interaction analysis. It is however important to underline the fact that the disordered histone tails play a role in the interactions with the DNA in the NCP. Yet, the mapping of such interaction networks would require using enhanced sampling methods, which is out of the scope of the present study.
In order to determine if the MD ensembles exhibit binding sites close to H3C110, pockets were tracked along the MD ensembles using the MDPocket software[42]. It was also interesting to scrutinize to what extent histone H3 sulfenylation and nitrosylation would influence binding sites on the nucleosome core particle architecture, because these two modifications are thought to be precursors for H3C110 S-glutathionylation by reaction with glutathione (a pseudo-tripeptide see Figure S1), but could also modulate binding sites on the NCP for partner proteins. Analyses were performed on the control system (1KX5) and on the modified ones (1KX5+SNO and 1KX5+SOH), and specific descriptors (pocket volume, hydrophobicity, etc.) were monitored for the pockets located near H3C110 and H3'C110.

Results and Discussion

S-sulfenylation perturbs DNA dynamics at the dyad and at the entry/exit point

To probe the effect of S-sulfenylation and S-nitrosylation on nucleosomal DNA stability, a PCA-based DNA dynamics analysis was performed on the generated MD ensembles, revealing that these buried modifications can impact DNA movements in two regions of interest - see Figure 2.

A major increase of the DNA dynamics is observed at its entry/exit site, in an asymmetric manner. This effect spans on the 15 terminal base-pairs for both S-sulfenylation and S-nitrosylation, yet the effect is less pronounced for the latter - see Figure 2a-c. This is correlated to the sampling of conformations that feature breathing/unwrapping processes of the DNA gyre extremity. Importantly, such asymmetry of DNA unwrapping has been observed experimentally and theoretically in the nucleosome[43,44], and are also linked to rearrangements in the histone core which plasticity is essential to allow for unwrapping processes[45]. We quantified these breathing motions using two descriptors: a dihedral angle ϕ (SHL0-SHL-2-SHL5-SHL7) illustrating an opening in the plane of the NCP, and a θ angle (SHL0-SHL5-SHL7) characterizing an out-of-plane deviation - see Figure 2-d. The distribution of these angles with respect to the control system highlights the sampling of conformations with a strongly pronounced opening upon S-sulfenylation, with ϕ values up to 80° ($\sim$34° in the control) and θ values up to 75 ° ($\sim$36° in the control) - see Figure 2-e. Upon S-nitrosylation, these angles do not reach peak values as high as for S-sulfenylation (max $\sim$55° for both ϕ and θ), yet their distribution highlights the non-negligible DNA breathing it can induce. It is important to note that these effects are observed on 2μs timescales, while such dynamical events could be captured only after 5-15μs simulations in the extensive canonical nucleosome study by Armeev et al.[23].

Another important effect is the increase of DNA dynamics at the dyad (around SHL0) induced by the S-sulfenylation - see Figure 2-a and c. This key-position of the DNA on the NCP generally features the most stable histone-DNA interactions, also driving DNA positioning onto the histone core. Upon S-sulfenylation, a destabilization of this generally very stiff location is observed for base pairs 68 to 83 and peaks at SHL$\pm$0.5, which is not observed for

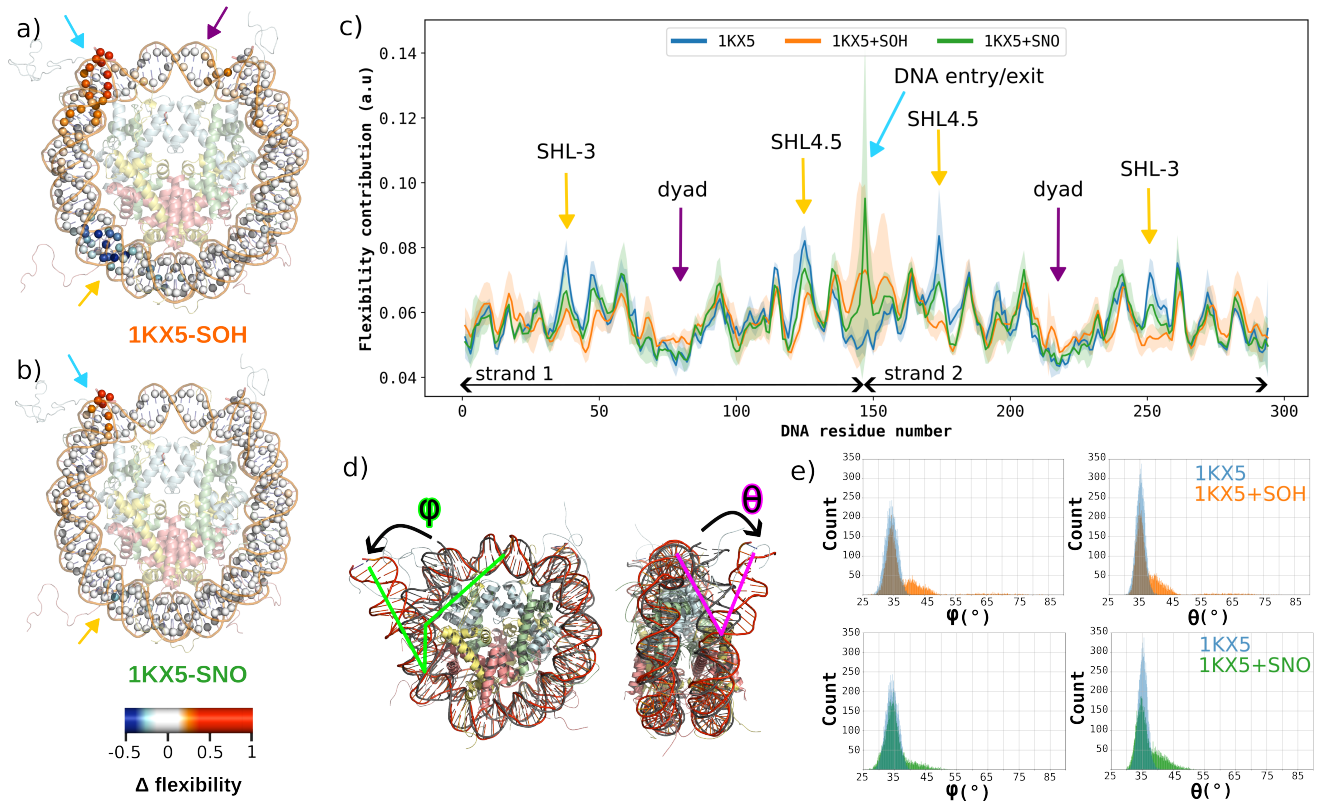

Fig. 2 a) Deviations of the DNA flexibility projected onto the NCP structure for the S-sulfenylated system (1KX5+SOH) with respect to the control system (1KX5), and b) for S-nitrosylation (1KX5+SNO) with respect to the control system. Tha decrease of flexibility is depicted in blue while and the increase appears in red. Arrows highlight the regions showing the highest deviations, colored to match the ones in panel c. c) Profiles of per residue flexibility contribution for DNA in the S-sulfenylated (orange), S-nitrosylated (green) and control (blue) systems. Regions where deviations are observed and SHL positions (dyad = SHL0 and DNA entry/exit = SHL7 here) are labeled by colored arrows. d) Scheme of the ϕ dihedral angle and the *theta* angle that were monitored to characterize DNA breathing. e) Distribution of the *phi* and *theta* angles for control (in blue), S-sulfenylated (in orange, top) and S-nitrosylation (in green, bottom) systems.

S-nitrosylation. While this effect may seem quantitatively mild compared to the deviations observed at the DNA entry/exit point, it is important to underline that SHL0 is usually the most stable region of the nucleosome and is associated with the lowest values and deviations for DNA flexibility in the control system - see Figure 2-c. A perturbation of the dynamics in this region may have a strong impact on the stability of the entire architecture. In a previous study, we actually show that hyperoxidation of H3C110 can destabilize this region and promote local sliding events of the DNA[21]. While we do not observe any sliding event with S-sulfenylation, the perturbation of the DNA dynamics at the dyad resembles very much to what we described in this other study - see Figure S2. The destabilization of DNA at the dyad by post-translational modifications is a hallmark of remodeling events such as DNA sliding and NCP disassembly[46], suggesting that H3C110 oxidation by S-sulfenylation and its higher order oxidative derivatives[21] might play a role in the promotion of these dynamical events.

Nucleosomal DNA dynamics may also be influenced by the conformational behavior of histone tails[47]. A closer look to the dynamics of each tail in the simulations shows that the differences of DNA flexibility characterized for S-sulfenylation and S-sulfonylation are not correlated to specific binding modes of the H3 histone tails in this region - see Figure S3. While in the simulations with S-sulfenylation there is no contact between the H3/H3' tails and DNA at the dyad, we can observe such interactions in the control, the S-nitrosylated and the S-sulfonylated systems (data taken from MD simulations of our previous work[21]). Thus, the increase in flexibility of the DNA helix at the dyad can not be correlated to the difference of H3 tails-DNA contacts in this region, as S-sulfenylation and S-sulfonylation both provoke an increase of DNA flexibility at the dyad but show dissimilar H3/H3'-DNA interaction patterns. The H4/H4' and H2A/H2A' conformations are not highly perturbed by the presence of any modification (S-sulfenylation, S-nitrosylation or S-sulfonylation) - see Figures S4 and S5. However, the H2B/H2B' tails conformations exhibit a more fluctuating conformational behavior in S-sulfenylation and S-nitrosylation compared to the control - see Figure S6. While in the present study the H2B tails are full length, the control system taken from our previous study[21] lacks the terminal PEP residues. This might have a role in the difference of DNA dynamics in the SHL-3/SHL4.5 regions which is observed for S-sulfenylated and S-nitrosylated systems - see Figure 2-a to c.

Noteworthy, the flexibility of the histone proteins do not show significant deviation from the control upon cysteine oxidation - see Figure S2. Likewise, the monitoring of DNA descriptors by

Curves+ did not reveal any significant perturbation of the helix structure compared to the control system, except for slightly larger deviations of the base-pair parameters at the dyad - see Figures S7-S9. Yet, these effects are mild, suggesting that while the dynamics of the DNA helix can be impacted by oxidative modification of the histone H3, the integrity of its helical structure is overall conserved.

Cysteine oxidation re-shapes the nucleosome intrinsic communication network

We recently showed how H3C110 hyperoxidation can induce a re-shaping of the histone core intrinsic architecture[21] using the COMMA2 software[48]. Since then we have released a new tool, COMPASS, allowing for the exploration of communication networks including not only proteins but also nucleic acids[49]. Here, we resorted to the latter approach to assess the effect of S-sulfenylation and S-nitrosylation on communication pathways within the entire NCP. Noteworthy, we also performed a COMMA2 analysis to allow for a direct comparison with the analysis of S-sulfonylation - see Figure S10 and full details in SI.

The computed communication pathways reveal a dense network that spreads throughout the whole nucleosome structure - see Figure 3-a. Histone H3 contains many of the most important communication hubs, especially on its α2 (E94, L109, I112, H113) and αN helices (L48, Q55, T58). At the dyad, H3K115, H3R116 and H3T118 are connected to a unique DNA base pair, and dense pathways also locally bridge DNA to histones at SHL$\pm$1.5 (via H3R63 and H3L65), SHL$\pm$2.5 (via H3R72 and H3R83), and SHL$\pm$3.5 (via H4K77 and H2BR83). Interestingly, the SHL closer to the DNA entry/exit points are less connected to the histone core, which might be important to allow the DNA unwrapping. Actually, we observe that only the very end of the helix on one side of the nucleosome (SHL6.5) is strongly connected to histones through H2A C-terminal tail and H3 αN helix. This asymmetric communication might have a role in the asymmetry observed during DNA unwrapping.

The S-sulfenylation of H3C110 provokes a pronounced rewiring of this communication network, especially regarding pathways bridging histones and DNA - see Figure 3-a. Indeed, the pathways here connect histones to DNA from SHL0 to SHL5.5 without discontinuity and are lost in the SHL6.5 region, which correlates with the DNA unwrapping observed in this region. S-sulfenylation induces an equilibrium of the native communication network, with marked differences in the dyad region, where a loss of pathways at SHL-0.5 is balanced by an increased communication at SHL0.5. The local destabilization of the DNA observed at the latter location might thus result from this rewiring of communication pathways, which also highlights how long-range effects can be induced by H3C110 S-sulfenylation.

Interestingly, S-nitrosylation has a much lesser impact on the communication network and shows an overall decrease of the pathways intensity. Only a few pathways are found to be enhanced in this case, that are located at the contact surface between H4 and H2B only on the side of the modification. This specific re-organization suggests a different functional role of this modification compared to S-sulfenylation.

A specific region of histone H3, spanning from H3H39 to H3R49, has been previously described to act as a latch holding together the DNA end (SHL$\pm$6-7) and the DNA near the dyad (SHL$\pm$0-1), whose perturbation would be linked to DNA unwrapping processes[23] - see Figure 3-c. The analysis of the cliques characterized by ComPASS reveals that cysteine oxidation, and in particular S-sulfenylation, allosterically destabilizes this H3-latch. Cliques are groups of residues that are fully connected within the graph and are likely to play pivotal roles in maintaining the functional dynamics of a given system. In the canonical NCP, we identified large cliques that correspond to the H3-latch, bridging the SHL$\pm$6-7 to SHL$\pm$0-1 - see Figure 3-d. These cliques involve the top of the histone H3 αN helix, i.e. residues T45 to R49, and the last residue of its tail, i.e. residues K37 to G44. Upon S-sulfenylation, these cliques do not bridge the two DNA gyres anymore but only the H3 residues to either SHL$\pm$0-1 or SHL$\pm$6-7 - see Figure 3-e. Interestingly, the H3 αN helix residues are less involved in these cliques, especially on the side of the NCP that undergoes large unwrapping in the simulations (latch 1 between SHL-0.5 and SHL6.5). The effect of S-nitrosylation on the H3-latch interactions with DNA is less pronounced than for S-sulfenylation, yet the H3 αN helix is also less involved in bridging cliques on both sides of the NCP. This effect is also visible from the analysis of the computed communities, that shows a separate community gathering the H3-latch and the DNA gyres at SHL$\pm$0.5 and SHL$\pm$6.5 in the control, which is lost upon S-sulfenylation and S-nitrosylation - see Figure S11. These results suggest that the absence of T45-R49 residues of the H3 αN helix from the cliques in this region translates into the promotion of DNA unwrapping.

Cysteine oxidation alters native DNA-histone contacts

In the nucleosome core particle, an intense network of hydrogen bonds and salt bridges ensures the interaction between DNA and histone proteins, maintaining the stability of its overall architecture. We probed the effect of H3C110 S-sulfenylation and S-nitrosylation on this network by exhaustively monitoring the DNA-histones interactions along the MD ensembles of the control and modified NCPs.

Scrutinizing the DNA-histone core contacts in the control system, we retrieve a set of well-known interactions - see Figure S12. Near the dyad, H3/H3'K64 and H4/H4'S47 strongly interact with DNA. To a lesser extent, interactions involving H3/H3'K115 and H3K122 are identified. At the DNA entry/exit points, H3/H3'T45 interact with several nucleotides, as part of the H3-latch mentioned above. At SHL$\pm$3, H4/H4'K79 and K77 show very frequent contacts with DNA, and the well-known H3/H3'K56 interactions with DNA are also retrieved at SHL$\pm$6. Several canonical interactions of histone residues with the nucleobases are also observed: H3/H3'R83 at SHL$\pm$2.5, H4/H4'R45 at SHL$\pm$0.5, H2A/H2A'R42 at SHL$\pm$3.5, and H2A/H2A'R77 at SHL$\pm$5.5. Other very persistent DNA-histone interactions involving non-polar or non-charged amino acids were also pinpointed, providing a complete contact map between the histone core and the DNA gyres. Among

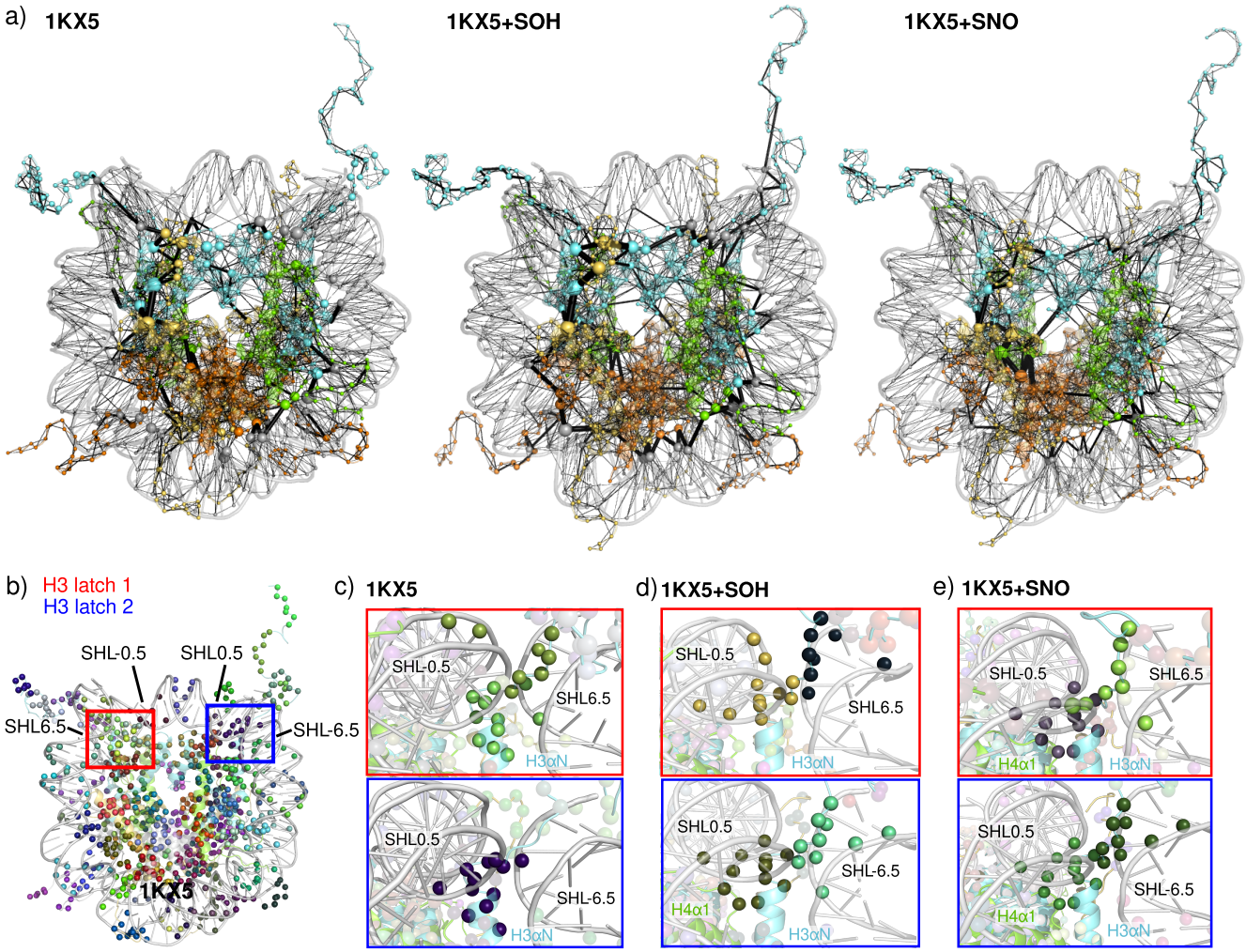

Fig. 3 a) Projection of the communication pathways calculated for the control (1KX5, left), the S-sulfenylation (1KX5+SOH, center), and the S-nitrosylted (1KX5+SNO, right) systems. The denser the pathway/hub, the larger the stick/sphere. b) Projection of the identified cliques, highlighting the position of the two H3 latch between DNA at SHL±0.5 and SHL±6.5 that influence DNA unwrapping. c) Zoom on the cliques corresponding to the H3 latches in the control system, d) in the S-sulfenylated system, e) in the S-nitrosylated system.

others, we pinpoint: alanines H3/H3'A47 and H2A/H2A'A45, glycines H3/H3'G44 and H4/H4'G48, and valines H3/H3'V46 and H3/H3'V116. Noteworthy, these interactions are all located between the SHL-1/SHL1 regions, near to the dyad. These hydrophobic residues might participate to the strong interaction network that makes the dyad the most strongly positioned part of the DNA in the NCP.

Upon oxidative modifications of H3C110, this interaction map is re-shaped - see Figure 4. For both S-sulfenylation and S-nitrosylation, we retrieve a decrease of prevalence for residues at the DNA entry/exit terminal base pairs that undergo unwrapping as above-described, strongly pronounced for base pairs 139 to 145. This seems to especially involve interactions with the residue H3T45, whose interaction prevalence drastically drops upon both S-sulfenylation (-33% with dG145 and -19% with dT144) and S-nitrosylation (-30% with dG145 and -15% with dT144). Interestingly, S-sulfenylation induces larger shifts of the per residue DNA-histone interactions prevalence than S-nitrosylation. It provokes a general decrease of interaction between DNA and the histone core. Besides the DNA extremity, a significant decrease of interaction near SHL0.5 is also observed, involving dC216, dA214, and dC82 (base pairs 79-82) in DNA, and residues H3'P43, H4'R39 and H4'R45 in histones. This perturbation of DNA-histone contacts is most probably involved in the above-described DNA destabilization observed in this region. Interestingly, we previously showed that H4'R45 interactions with the DNA is also perturbed by S-sulfonylation, which can allow local sliding events of the DNA helix[21]. In the case of S-sulfenylation no DNA sliding was characterized, but these observations still highlight possible common mechanisms underlying S-sulfenylation and S-sulfonylation effect on the NCP dynamics.

Importantly, changes in DNA/histone core interactions might not be enough to explain the lower DNA flexibility characterized at SHL4.5 and SHL-3 (see Figure 2), as in this region both increases and decreases of the interaction prevalence are observed. Indeed, while there is an increase of the prevalence to interact with DNA for H4K77 (+20%), H4K79 (+14%), H2A'H31 (+22%) and H2A'R32 (+13%), H2AR20 and H4R78 exhibit fewer contacts

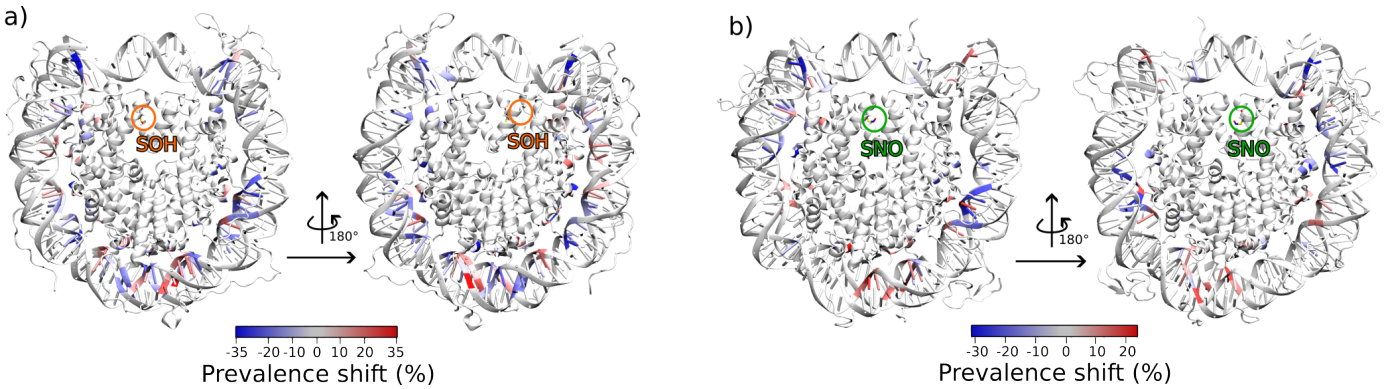

Fig. 4 Projection of the per residue DNA-histone interaction prevalence shift for a) the S-sulfenylated and b) the S-nitrosylated systems with respect to the control. Negative to positive shifts in DNA-histone interactions are depicted from blue to red. For sake of clarity, only shifts higher than 10% of prevalence are projected. Histone tails were excluded from the analysis. For each residue, the value displayed is the difference of prevalence to be involved in DNA-histone contacts between the modified system and the control one. The modified residues (SOH and SNO) are marked by orange and green circles, respectively.

with the nucleic acids (+10% and -29%, respectively). Here, the conformational behavior of the H2B tail, that protrudes from the NCP in this region, is found to be slightly different between the oxidized systems and the control (see Figure S6), which might influence local DNA dynamics.

Compared to S-sulfenylation, S-nitrosylation induces much less deviation from the control system - see Figure 4-b. In line with the difference of DNA flexibility profiles, the interaction prevalence of the DNA residues at the dyad is higher in the S-nitrosylated system than for S-sulfenylation, which is also the case for histone residues near SHL0.5. Some deviations are also noted in the area near H3α2 helix lower end, denoting a differential perturbation of the long-range communication pathways. For instance, the shift of interaction prevalence for H3S86 is positive with S-nitrosylation (+10%) and negative with S-sulfenylation (-31%). In the H3α1 helix, H3K64 interactions with DNA are weakened with S-nitrosylation (-32%) while strengthened with S-sulfenylation (+15%), which is also the case for H3R636 (-18% with S-nitrosylation and +21% with S-sulfenylation).

S-sulfenylation and S-nitrosylation have not effect on the accessibility of H3C110

Besides S-sulfenylation and S-nitrosylation, H3C110 has ben described to undergo S-glutathinylation *in vitro* and *in vivo*[18]. It is also known that S-sulfenylation and S-nitrosylation can act as intermediates towards S-glutathionylation, via activation of the cysteine to promote its reaction with glutathione. In the nucleosome, the highly buried character of H3C110 raises questions about the molecular mechanisms promoting the formation of its bulky S-glutathionylated derivative. In order to bring insights into the effect of S-sulfenylation and S-nitrosylation on the cysteine accessibility and the formation of binding pockets in its surroundings, we performed MDpocket analyses on the MD ensembles of 1KX5 (control), 1KX5+SOH (sulfenylation) and 1KX5+SNO (nitrosylation). The control system already exhibits a binding pocket near the H3C110 on both NCP sides (i.e., and symmetrically near H3'C110), mainly formed by residues H3L109, H3'L126,

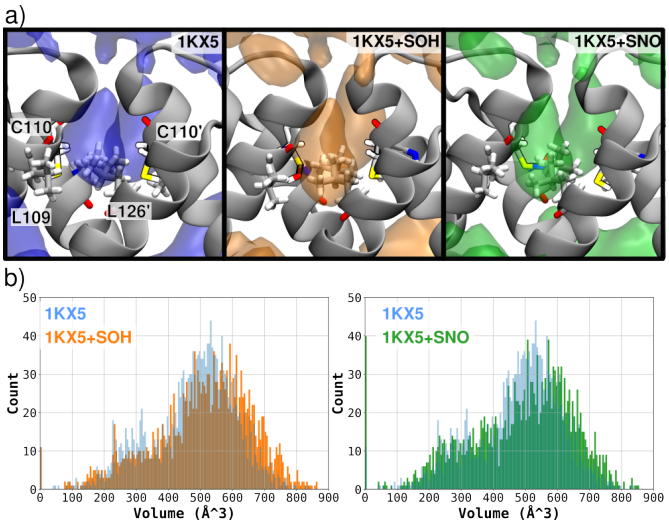

Fig. 5 a) Representation of the pockets characterized in the vicinity of H3C110, in MD ensembles from the control system (1KX5, blue, left), with S-sulfenylation (1KX5+SOH, orange, center), and with S-nitrosylation (1KX5+SNO, green, right). The hydrophobic residues shielding H3C110 and H3'C110 (L109 and L126 of each H3 copy) are depicted in licorice, as well as the two cysteines. b) Distribution of volume of the pockets near H3C110 and H3'C110 for control (in blue), S-sulfenylated systems (in orange, left) and S-nitrosylation systems (in green, right).

H3H113, H3L112, H3'K122 and H3'R129. While this could be the binding site for pre-reactive complexes of activated glutathione with H3C110 (e.g. GSNO[19]), hydrophobic residues (H3/H3'L109 and H3'/H3L126) still shield the cysteine, which remains hardly accessible. Of note, GSNO, which is a putative reactant towards S-glutathionylation, harbors negative charges on its termini which could interact favorably with the positively charged residue of the binding pocket near H3C110.

These symmetrical binding pockets are retrieved from the simulations with S-sulfenylation and S-nitrosylation, which only differ by the contribution of H3'R145 to the pocket, that exhibits a mildly larger volume - see Figure 5-b. However, the oxida-

tive modifications do not allow the modulation of the pocket shape to reach the cysteine for pre-reactive states precluding S-glutathionylation. The H3L09 adjacent to the modified cysteine and the facing H3'L126 remains stable and hinder any exposure of the reactive sulfur. A slight increase in the polarity and the charge scores of the pockets is observed in the oxidized system, concomitant with a mild decrease of hydrophobicity, which might render the binding site more favorable to glutathione and its derivatives - see Figure S1. Noteworthy, the pockets characterized on the overall NCP surface in the control system remain mostly unchanged upon S-sulfenylation and S-nitrosylation -see Figure S1.

While the two H3C110 oxidative modifications used in this study do not promote the accessibility of the cysteine in our simulations, one can not rule out the possibility of an exposure of the reactive sulfur induced by the binding with the glutathione derivative itself. The symmetrical pockets observed in the vicinity of H3C110 and H3'C110 might constitute a binding site for glutathione or its oxidized derivatives that could be the first step towards S-glutathionylation. Unraveling the mechanisms of the interactions between glutathione and the NCP will be the topic of future investigations. Beyond H3 glutathionylation, these binding pockets could be pivotal for other processes occurring in this region of the nucleosome, such as the recently characterized copper-reductase function of the H3-H4 tetramer[50].

Conclusions

Histone post-translational modifications are major regulators of the chromatin dynamics. They modulate the structure and dynamics of the nucleosome through fine tune mechanisms that modulate DNA compaction in a specific way. Here, we brought out new information about the impact of two oxidative histone H3C110 modifications, S-sulfenylation and S-nitrosylation, on a nucleosome core particle dynamics. Resorting to extensive MD simulations, we provide an all-atom description of the structural signature of these two PTMs, revealing that the chemical nature of the modification drives its effect on the NCP structure. While S-sulfenylation increases DNA unwrapping and DNA dynamics at the dyad, S-nitrosylation induces a milder perturbation of the NCP architecture, suggesting different functions for these two PTMs. We highlight allosteric effects driven by the modifications, that are transmitted through rewired communication pathways especially and impact DNA-histone interaction such as the H3 latch that has been linked to DNA unwrapping processes[23]. Importantly, the impact of S-sulfenylation on the NCP dynamics is similar to the one previously described for S-sulfonylation[21]. This suggests a differential effect of H3C110 oxidative PTM in the nucleosome depending on their chemistry: consecutive oxidation levels of the cysteine (S-sulfenylation/S-sulfonylation) might promote remodeling events involving the destabilization of interactions at the dyad (DNA sliding, NCP disassembly), while S-nitrosylation might not have any intrinsic effect but rather might act as an intermediate towards S-glutathionylation as suggested in the literature[51]. Experimental validation of this hypothesis would provide important insights to fully understand the functional role of these PTMs.

Besides, our results reveal the presence of a binding pocket near H3C110/H3'C110, which could be a docking site for reactants towards S-glutathionylation. However, the cysteine remains highly buried in our simulations, which suggests that its accessibility might be directly triggered by the binding of reactants in this area, which is a current matter of investigation in our lab. Noteworthy, this region of the NCP has also been described to catalyze copper reduction[50], in which the identified binding pocket might play a role.

Overall, we provide the first insights into the modulation of the NCP structure by histone oxidative PTMs, revealing the ability of S-sulfenylation to increase DNA dynamics at the dyad and at the DNA entry/exit site through allosteric mechanisms, that suggests a promoting role of this PTM for nucleosome disassembly. Experimental data would be needed to validate these observations and to fully understand how this PTM-induced reorganization of the nucleosome core particle can impact higher-order structures such as chromatin.

Author Contributions

Conceptualization and Project Administration: E.B.; Methodology and Resources: E.B., Y.K. and R.G-A; Data Curation, Visualization, Writing – Original Draft and Writing – Review & Editing: all authors.

Conflicts of interest

There are no conflicts to declare.

Data availability

Data for this article, including MD trajectories and a list of prevalence of DNA-histone contacts, are available on Zenodo at 10.5281/zenodo.15112932.

Acknowledgements

This work was performed using HPC resources from GENCI-IDRIS (Grant 2023-A0150714577) and EXPLOR (Grant 2019CP-MXX0983).

Notes and references

1 R. K. McGinty and S. Tan, *Chemical reviews*, 2015, **115**, 2255–2273.

2 N. Gillet, E. Dumont and E. Bignon, *Biophysical Reviews*, 2024, 1–12.

3 G. Millán-Zambrano, A. Burton, A. J. Bannister and R. Schneider, *Nature Reviews Genetics*, 2022, **23**, 563–580.

4 M. Simon, J. A. North, J. C. Shimko, R. A. Forties, M. B. Ferdinand, M. Manohar, M. Zhang, R. Fishel, J. J. Ottesen and M. G. Poirier, *Proceedings of the National Academy of Sciences*, 2011, **108**, 12711–12716.

5 J. A. North, S. Javaid, M. B. Ferdinand, N. Chatterjee, J. W. Picking, M. Shoffner, R. J. Nakkula, B. Bartholomew, J. J. Ottesen, R. Fishel *et al.*, *Nucleic acids research*, 2011, **39**, 6465–6474.

6 V. Di Cerbo, F. Mohn, D. P. Ryan, E. Montellier, S. Kacem, P. Tropberger, E. Kallis, M. Holzner, L. Hoerner, A. Feldmann *et al.*, *elife*, 2014, **3**, e01632.

7 S. Rizza and G. Filomeni, *Biochemical Journal*, 2020, **477**, 3649–3672.

8 D. T. Hess, A. Matsumoto, S.-O. Kim, H. E. Marshall and J. S. Stamler, *Nature reviews Molecular cell biology*, 2005, **6**, 150–166.

9 D. Seth, C. T. Stomberski, P. J. McLaughlin, R. T. Premont, K. Lundberg and J. S. Stamler, *Antioxidants & Redox Signaling*, 2023, **39**, 621–634.

10 P. Anand and J. S. Stamler, *Journal of molecular medicine*, 2012, **90**, 233–244.

11 H.-L. Zhou, Z. W. Grimmett, N. M. Venetos, C. T. Stomberski, Z. Qian, P. J. McLaughlin, P. K. Bansal, R. Zhang, J. D. Reynolds, R. T. Premont *et al.*, *Cell*, 2023, **186**, 5812–5825.

12 G. Roos and J. Messens, *Free Radical Biology and Medicine*, 2011, **51**, 314–326.

13 A. E. Beedle, S. Lynham and S. Garcia-Manyes, *Nature communications*, 2016, **7**, 12490.

14 Y. Song, Z. Xu, Q. Zhong, R. Zhang, X. Sun and G. Chen, *Frontiers in Pharmacology*, 2023, **14**, 1303465.

15 C.-Y. Yang, C.-F. Yang, X.-F. Tang, L. E. Machado, J. P. Singh, W. Peti, C.-S. Chen and T.-C. Meng, *Free Radical Biology and Medicine*, 2023, **194**, 147–159.

16 Y. Ma, M. Yi, W. Wang, X. Liu, Q. Wang, C. Liu, Y. Chen and H. Deng, *Cell Death & Disease*, 2022, **13**, 944.

17 J. L. García-Giménez, C. Romá-Mateo and F. V. Pallardó, *Biofactors*, 2019, **45**, 641–650.

18 J.-L. García-Giménez, C. Garcés, C. Romá-Mateo and F. V. Pallardó, *Free Radical Biology and Medicine*, 2021, **170**, 6–18.

19 J. L. García-Giménez, G. Olaso, S. B. Hake, C. Bönisch, S. M. Wiedemann, J. Markovic, F. Dasi, A. Gimeno, C. Pérez-Quilis, O. Palacios *et al.*, *Antioxidants & redox signaling*, 2013, **19**, 1305–1320.

20 A. De Luca, N. Moroni, A. Serafino, A. Primavera, A. Pastore, J. Z. Pedersen, R. Petruzzelli, M. G. Farrace, P. Pierimarchi, G. Moroni *et al.*, *Biochemical Journal*, 2011, **440**, 175–183.

21 Y. Karami and E. Bignon, *Computational and Structural Biotechnology Journal*, 2024, **23**, 1387–1396.

22 G. A. Armeev, A. K. Gribkova, I. Pospelova, G. A. Komarova and A. K. Shaytan, *Current Opinion in Structural Biology*, 2019, **56**, 46–55.

23 G. A. Armeev, A. S. Kniazeva, G. A. Komarova, M. P. Kirpichnikov and A. K. Shaytan, *Nature communications*, 2021, **12**, 2387.

24 E. A. Morrison, L. Baweja, M. G. Poirier, J. Wereszczynski and C. A. Musselman, *Nucleic acids research*, 2021, **49**, 4750–4767.

25 M. A. Öztürk, M. De, V. Cojocaru and R. C. Wade, *Annual review of physical chemistry*, 2020, **71**, 101–119.

26 J. Huertas and V. Cojocaru, *Journal of molecular biology*, 2021, **433**, 166744.

27 Y. Peng, D. Espiritu, S. Li, D. Landsman and A. Panchenko, *Biophysical Journal*, 2022, **121**, 361a.

28 W. Humphrey, A. Dalke and K. Schulten, *J. Mol. Graph.*, 1996, **14**, 33–38.

29 Schrödinger, LLC.

30 C. A. Davey, D. F. Sargent, K. Luger, A. W. Maeder and T. J. Richmond, *Journal of molecular biology*, 2002, **319**, 1097–1113.

31 J. A. Maier, C. Martinez, K. Kasavajhala, L. Wickstrom, K. E. Hauser and C. Simmerling, *Journal of chemical theory and computation*, 2015, **11**, 3696–3713.

32 I. Ivani, P. D. Dans, A. Noy, A. Perez, I. Faustino, A. Hospital, J. Walther, P. Andrio, R. Goni, A. Balaceanu, G. Portella, F. Battistini, J. L. Gelpí, C. González, M. Vendruscolo, C. A. Laughton, S. A. Harris, D. A. Case, and M. Orozco, *Nature Methods*, 2016, **38**, 55–58.

33 J. Yoo and A. Aksimentiev, *Physical Chemistry Chemical Physics*, 2018, **20**, 8432–8449.

34 S. Han, *Biochemical and biophysical research communications*, 2008, **377**, 612–616.

35 C. W. Hopkins, S. Le Grand, R. C. Walker and A. E. Roitberg, *Journal of Chemical Theory and Computation*, 2015, **11**, 1864–1874.

36 C. Balusek, H. Hwang, C. H. Lau, K. Lundquist, A. Hazel, A. Pavlova, D. L. Lynch, P. H. Reggio, Y. Wang and J. C. Gumbart, *Journal of chemical theory and computation*, 2019, **15**, 4673–4686.

37 T. Darden, D. York and L. Pedersen, *The Journal of chemical physics*, 1993, **98**, 10089–10092.

38 E. Bignon, N. Gillet, T. Jiang, C. Morell and E. Dumont, *The Journal of Physical Chemistry Letters*, 2021, **12**, 6014–6019.

39 E. Bignon, V. E. Claerbout, T. Jiang, C. Morell, N. Gillet and E. Dumont, *Scientific reports*, 2020, **10**, 17314.

40 R. Lavery, M. Moakher, J. H. Maddocks, D. Petkeviciute and K. Zakrzewska, *Nucleic Acids Research*, 2009, **37**, 5917–5929.

41 C. Bouysset and S. Fiorucci, *Journal of Cheminformatics*, 2021, **13**, 72.

42 P. Schmidtke, V. Le Guilloux, J. Maupetit and P. Tuffi¿ 1/2ry, *Nucleic acids research*, 2010, **38**, W582–W589.

43 H. Kono and H. Ishida, *Current Opinion in Structural Biology*, 2020, **64**, 119–125.

44 O. Ordu, A. Lusser and N. H. Dekker, *Biophysical reviews*, 2016, **8**, 33–49.

45 S. Bilokapic, M. Strauss and M. Halic, *Nature structural & molecular biology*, 2018, **25**, 101–108.

46 G. D. Bowman and M. G. Poirier, *Chemical reviews*, 2014, **115**, 2274–2295.

47 S. Morioka, T. Oishi, S. Hatazawa, T. Kakuta, T. Ogoshi, K. Umeda, N. Kodera, H. Kurumizaka and M. Shibata, *Nano Letters*, 2024.

48 Y. Karami, T. Bitard-Feildel, E. Laine and A. Carbone, *Scientific reports*, 2018, **8**, 16126.

49 S. Bheemireddy, R. González Alemán, E. Bignon and Y. Karami, *bioRxiv*, 2025, 2025–02.

50 N. Attar, O. A. Campos, M. Vogelauer, C. Cheng, Y. Xue, S. Schmollinger, L. Salwinski, N. V. Mallipeddi, B. A. Boone, L. Yen *et al.*, *Science*, 2020, **369**, 59–64.

51 E. Kalinina and M. Novichkova, *Molecules*, 2021, **26**, 435.